

# A Minimalistic, Synthetic Cell-Inspired Metamaterial for Enabling Reversible Strain-Stiffening

Mohammadreza Taale, Målin Schmidt, Fereydoon Taheri, Michael Timmermann, and Christine Selhuber-Unkel\*

**Strain-stiffening, i.e. the nonlinear stiffening of a material in response to a strain, is an intrinsic feature of many biological systems, including skin, blood vessels, and single cells. To avoid a mismatch in mechanical properties, synthetic materials in contact with such biological systems should also be strain-stiffening. Conventional strain-stiffening materials are either highly dependent on the applied strain-rate, or only available for a limited stiffness regime. Both aspects limit the applicability of these materials. In contrast, living cells employ a dynamic strain-stiffening mechanism that is based on the cross-linking of cytoskeletal fibers in response to external stress. This strain-stiffening of the cytoskeleton is mimicked in a mechanical metamaterial by a minimalistic structure consisting of parallel slats connected to backbones. Herein, it is demonstrated experimentally that the structures can be adapted such that the strain required for stiffening, the final stiffness, as well as the degree of stiffening can be tuned, particularly by combining several strain-stiffening elements. These properties make the structure promising for the development of devices that should resemble the mechanical properties of human soft tissues, e.g., skin-integrated flexible electronics and blood vessel grafts.**

such strategy to protect biological systems from damage. Examples of biological systems that are mechanically strain-stiffening include blood vessels,<sup>[2]</sup> skin,<sup>[3]</sup> and lung tissue,<sup>[1]</sup> to name a few. In all devices that are constantly in touch with such tissues the strain-stiffening effect should be considered to avoid mechanical mismatch, which can have dramatic consequences in implants. An important example is intima hyperplasia, which can lead to poor patency of small diameter synthetic vascular grafts.<sup>[5]</sup> The mechanical matching of device and skin is also an essential prerequisite for the functionality of electronic skin applications.<sup>[6]</sup>

Whereas many soft materials demonstrate stiffening in response to compression force, the study and development of materials that demonstrate stiffening in response to tensile force is much more limited. Most approaches directly modify the material matrix, for example by introducing nanocrystals into a hydrogel matrix.<sup>[7]</sup> Chemically-induced

## 1. Introduction

Biological systems have evolved smart strategies to cope with physical forces.<sup>[1]</sup> Strain-stiffening, which describes the nonlinear stiffening of a material in response to external stress, is one

strain-stiffening can also arise from strain-induced active cross-linking in networks of synthetic polymers. For example, Yan et al. presented gels where a Schiff base reaction between the amino groups and aldehyde groups on poly(ethylene glycol) and branched polyethylenimine reversibly cross-link upon elongation of the gel, causing reversible strain-stiffening.<sup>[8]</sup> Also, supramolecular zwitterionic networks have proven valuable.<sup>[9]</sup> The stiffness of these gels is in the lower kPa region, making it, similar to the materials described before, suitable for tissue engineering and synthetic skin applications. Bioinspired strain-stiffening approaches also include intertwined nanofibrils composed of short alkyl side chain-modified polymer chains, to mimic the crimped structure of collagen,<sup>[10]</sup> DNA nanoswitches to control the stiffness of hydrogels,<sup>[11]</sup> and in chitosan-based self-healing hydrogels<sup>[12]</sup>. Furthermore, also microgel-based approaches have been reported to serve as biomimetic strain-stiffening materials.<sup>[13]</sup> However, the abovementioned strategies require chemically modified materials that are not easily available for standard and macroscopic applications. In addition, fabric materials can be structured such that they are strain-stiffening, but reversibility often does not occur and hysteresis can be observed.<sup>[14]</sup>

Whereas many synthetic materials do not demonstrate strain-stiffening behavior,<sup>[15]</sup> we can take inspiration from biology.

M. Taale, M. Schmidt, F. Taheri, C. Selhuber-Unkel  
Institute for Molecular Systems Engineering and Advanced Materials (IMSEAM)  
Heidelberg University  
69120 Heidelberg, Germany  
E-mail: selhuber@uni-heidelberg.de  
M. Timmermann  
Institute for Materials Science  
Kiel University  
24143 Kiel, Germany

 The ORCID identification number(s) for the author(s) of this article can be found under <https://doi.org/10.1002/admt.202201441>

© 2023 The Authors. Advanced Materials Technologies published by Wiley-VCH GmbH. This is an open access article under the terms of the Creative Commons Attribution License, which permits use, distribution and reproduction in any medium, provided the original work is properly cited.

DOI: 10.1002/admt.202201441

Simple biological systems, e.g., fibroblast cells from the connective tissue, have an intriguing way of strain-stiffening. Cytoskeletal components, mainly actin, which allows cells to react actively to external force, play a main role as they structurally rearrange the actin filament network to form strongly cross-linked actin stress fibers during adhesion,<sup>[16]</sup> which are in turn connected to focal adhesion clusters. The formation of actin stress fibers can be induced by an external stimulus, for example in endothelial cells and fibroblasts as a response to the pulsatile stretching.<sup>[17]</sup> It has been shown that this formation of stress fibers increases cell stiffness<sup>[18]</sup> and that stress fibers are actively reinforced and repaired in response to external forces.<sup>[19]</sup> Stress fibers are made up from bundles of  $\approx 10$ – $30$  actin filaments, where  $\alpha$ -actinin serves as a cross-linker of the filaments.<sup>[20]</sup>

Here, we present a minimalistic, purely synthetic approach to mimic the principle of the cross-linking of actin filaments stress fibers in a silicone-based metamaterial by slats that are “cross-linked” through contact. Polydimethylsiloxane (PDMS) is an excellent silicone material for such studies as its stiffness can be tuned and it can be easily shaped by molding.<sup>[21]</sup> Hence, we fabricated slats in a defined structure. Our work demonstrates that the strain-stiffening of our PDMS-metamaterial is independent of the strain-rate and lubricants, and its mechanical properties are highly tunable and directional. We also include a demonstration of its applicability for damping the free fall of weights.

## 2. Results and Discussion

To achieve a strain-stiffening minimalistic metamaterial, we mimic the formation of actin stress fibers by cross-linking of actin filaments. In **Figure 1A**, actin stress fiber formation in cells in response to the application of strain is roughly sketched. In our cell-inspired structure (**Figure 1B**), the actin filaments are replaced by elastic slats that are attached to bars at equal distances. Upon strain application, the slats deform and touch each other at a critical strain, thereby mimicking the cross-linking of filaments in cells. Whereas energy is initially dissipated by the bending of the individual slats, the slats coming into contact leads to a stretch of the material in a bulk-like configuration. Thus, the contact between the slats mimics the cross-linking of actin filaments in actin stress fibers and thus leads to an increase in overall stiffness.

**Figure 1C** shows the strain-stiffening unit made up of two of the simple structures shown in **Figure 1B**. This symmetric structure has been chosen to simplify tensile testing and applications. A large number of different parameters can be defined and their effect was systematically tested. Four slat elements, each containing ten parallel elastic slats, are located between two outer backbones and two middle backbones (**Figure 1C**). Variations of this design can be made by parameter changes in the backbone height  $h$ , the number of slats per set  $N$ , slat-length  $l$ , slat-width  $w$ , the distance between slats  $d$ , sample depth  $D$ , protrusion length  $p/p'$ , and the gap between sets of slats  $g$ . All parameters have distinctive functions for the strain-stiffening behavior and by altering their size, the strain-stiffening behavior can be finely tuned to achieve the desired stiffness properties.

To investigate the mechanical properties of this strain-stiffening unit (**Table 1**) experimentally, we carried out uniaxial tensile testing of samples from highly elastic PDMS. The PDMS

used (Elastosil RT625, Wacker, Germany) has a tear strength of up to strains of 600%. We only elongated up to a strain of 60% to ensure that all experiments were carried out in the Hookean regime. **Figure 2** shows the deformation of a strain-stiffening unit during a tensile test and the resulting force curve in the tensile test. After a certain deformation, the slats start to touch each other (**Supporting Movie S1**). By further increasing the strain, greater surface contact is acquired to a point where almost every slat has established a maximum contact surface with the adjacent one. Consequently, the stiffness of the structure increases. We call this regime the transition regime. The transition regime denotes the part of the force-strain curve that shows a non-linear behavior. This can be explained by a formation of a quasi-bulk state at the area they touch that increases with further deformation. At a certain point, the contribution of the backbone exceeds that of the slats so that the mechanical behavior of the structure is governed by the stiffness of the backbone. This marks off the end of the transition state and the regime of final stiffness is reached. With further deformation, the contact area between the slats increases up to a point where more deformation mainly leads to an elongation of the backbones. This results again in a linear force-strain behavior, which defines the final stiffness.

To further demonstrate that the mechanical features of the metamaterial indeed are an intrinsic feature of its cell-inspired structure, we investigated the properties of an unstructured sample, but otherwise identical parameters (**Figure 2A**). Clearly, the reference curve does not exhibit strain-stiffening, whereas the strain-stiffening unit led to a stiffness increase at a critical strain of 30%. As in the strain-stiffening unit, energy is dissipated for bending the individual slats, the initial stiffness of the strain-stiffening unit is smaller than that of the unstructured unit. The final stiffness of the strain-stiffening unit ( $(0.74772 \pm 0.0006)$  N/mm) is similar to that of the unstructured sample ( $(0.80596 \pm 0.0003)$  N/mm). This final stiffness defines the maximum possible stiffness for this metamaterial. To prove the directionality of strain-stiffening, we also changed the orientation of the slats with respect to the pulling direction. No strain-stiffening was observed for this other slat orientation (**Figure S1**, **Supporting Information**). To demonstrate the versatility of our purely structural (not chemical) approach, we have also used a PDMS-carbon-composite material instead of PDMS and demonstrated the strain-stiffening effect in this sample (**Figure S2**, **Supporting Information**).

To investigate the impact of different structural parameters on the mechanical properties of the strain-stiffening unit (**Figure 1C**), we carried out tensile tests on such units with different slat width, slat length, slat distance, and backbone height. A detailed analysis of these results is shown in **Figure 3**, where we relate the degree of stiffening to the different parameters. We estimated the initial and final stiffnesses by fitting a simple linear regression model to the curve at strain level of  $\sim 7\%$  to  $20\%$  for the initial stiffness and  $\approx 30\%$  to  $47\%$  for the final stiffness.

As shown in **Figure 3A–D**, the main results of these experiments are: A variation of the backbone height  $h$  influences the final stiffness of the unit. An increase in the backbone height mainly leads to an increase in the final stiffness (**Figure 3A**). Additionally, a slight increase in the initial stiffness can be observed. Varying the backbone height influence neither the initial stiffness nor the critical strain. This confirms that the initial stiffness is

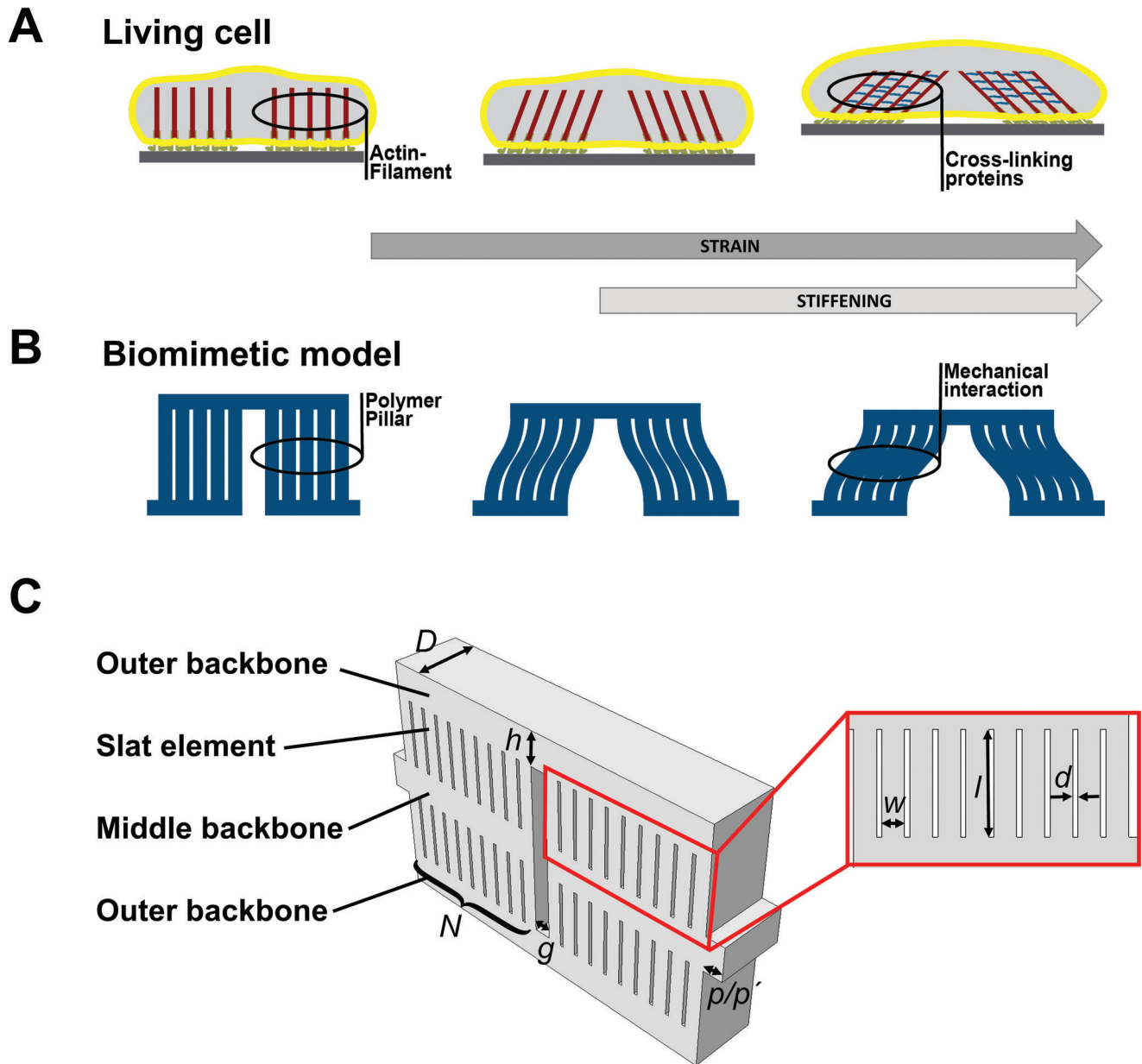


**Figure 1.** Sketch of the cell-inspired principle of our strain-stiffening structure. A cell is attached to a surface A). If the surface underneath the cell is strained, actin filaments (red) interconnect by cross-linking proteins (blue). The resulting actin stress-fibers increase the overall stiffness of the cell in a reversible way. In our cell-inspired strain-stiffening structure B) the principle of actin cross-linking is transferred into a minimalistic synthetic design, where elastic slats mimic the actin fibers. Upon strain application, the slats deform and eventually touch each other. This contact causes a change in the mechanical properties of the structure, which in turn leads to stiffening. The design consists of three main parts C): Two outer backbones, two middle backbones, and four blocks of each 10 parallel slat elements. Variations within this design geometry can be made by parameter changes in the backbone height  $h$ , the number of slats per set  $N$ , slat-length  $l$ , slat-width  $w$ , the distance between slats  $d$ , sample depth  $D$ , protrusion length  $p/p'$ , and the gap between sets of slats  $g$ .

mainly governed by the bending of slats rather than the stretching of the backbone as the backbones have a greater spring constant.

An increase in the slat length  $l$  influences the stiffness of the structure inversely, leading to a significant decrease in the initial stiffness, and a slight increase in the final stiffness (Figure 3B). Due to the connection to the backbone and the material proper-

ties, the slats deform into an S-shape curve Figure 2B. A sharper S-shape bend is required when using a short slat length than when using a longer slat length for devices stretched the same distance, and a greater proportion of the slat is deformed when the slat length is short than when the slat length is long for devices stretched the same distance. As a result, an increase in the slat length  $l$  influences the stiffness of the structure inversely.

**Table 1.** Parameters used for the strain-stiffening unit.

Parameters	Variables	Values
Backbone height	$h$	5 mm
Slat-length	$l$	10 mm
Slat-width	$w$	2.1 mm
Slats distance	$d$	0.5 mm
Number of slats	$N$	10
Sample-depth	$D$	10 mm
Protrusion-length (tensile test)	$p$	15 mm
Protrusion-length (FEM)	$p'$	2.75 mm
Gap between sets of slats	$g$	2.5 mm

When using longer slats rather than shorter slats, there will be a decreased initial stiffness and a lower force will be required for bending the slats from their resting state. A special case is shown when the slat length is decreased to 8 mm. At this point, the slat length is too short to properly form the S-curve required for strain-stiffening behavior, and the stiffness of the slats is comparable to the stiffness of the backbone.

An increase in slat distance  $d$  causes more stretching to be required before the slats come into contact, resulting in a shift of the critical strain toward higher strains (Figure 3C). The slight increase of initial and final stiffness with decreasing slat distance is caused by an increase in backbone stiffness, as its stiffness scales

inversely with slat length and a decrease of slat distance causes a decrease in backbone length (unless the number of slats is increased). The moment the slats come into contact during deformation determines the position of the transition regime, as observed by the influence of varying slat width. The initial and final stiffness both decrease drastically by a small reduction in slat width. This occurs because the decrease in slat width results in a lower bending moment, leading to lower stiffness (Figure 3D). The critical stiffness stays unchanged though.

All these features can be tailored and enhanced to suit a specified need in a particular application by in-series and parallel arrangements of strain-stiffening elements (Figure 4). The strain-stiffening units in an in-series and a parallel arrangement are connected end-to-end and side-by-side via the protrusions or backbones, respectively. When two strain-stiffening units are in series, any force applied to the ensemble gets applied to each unit without a change of magnitude. The transition regime of the in-series arrangement occurs at 30% strain, but on different total elongation lengths (Figure 4C). The transition regime of the parallel arrangement occurs at almost the same strain ( $\approx 30\%$ ) but at  $\approx 6$  N, which is double the force of a single unit. This agrees with the in-series / parallel equivalent spring law. Therefore, the equivalent stiffness follows the equations  $E_e = \sum_{n=1}^{\infty} (\frac{1}{E_n})$  for parallel arrangement and  $E_e = \sum_{n=1}^{\infty} (E_n)$  for serial arrangement, where  $E_e$  is the equivalent stiffness and  $E_n$  is the stiffness of each unit. This

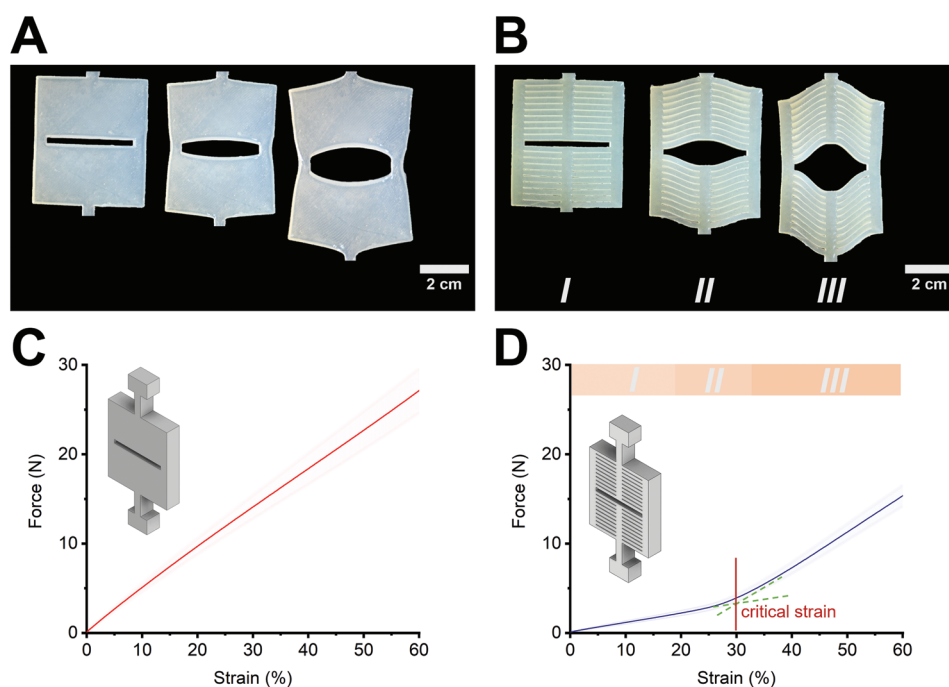


**Figure 2.** Straining a PDMS strain-stiffening unit and respective force-strain-curve. A) Shape change of an unstructured unit. B) Shape change of the strain-stiffening unit during a tensile test. C) Force-strain-curve of the unstructured element, lacking strain-stiffening. D) Force-strain-curve of the strain-stiffening unit. In the stress-strain-curve three stiffness regimes can be identified: The initial stiffness (I), dominated by the bending of individual slats. The transition stiffness (II), is not a constant and determines the transition between the initially soft material to the stiffened material. And the final stiffness (III), which represents the final, stiffened situation where the slats touch each other. The critical strain is defined as the intersection of the linear stress-strain curve for the initial stiffness, and the one of the final stiffness. Two protrusions with T-shaped endings are added on both sides of the structure which help as clamping spots in a tensile test setup. The standard deviation is illustrated as the margin for each graph. For each condition, 3 different samples were measured (3 force curves each).

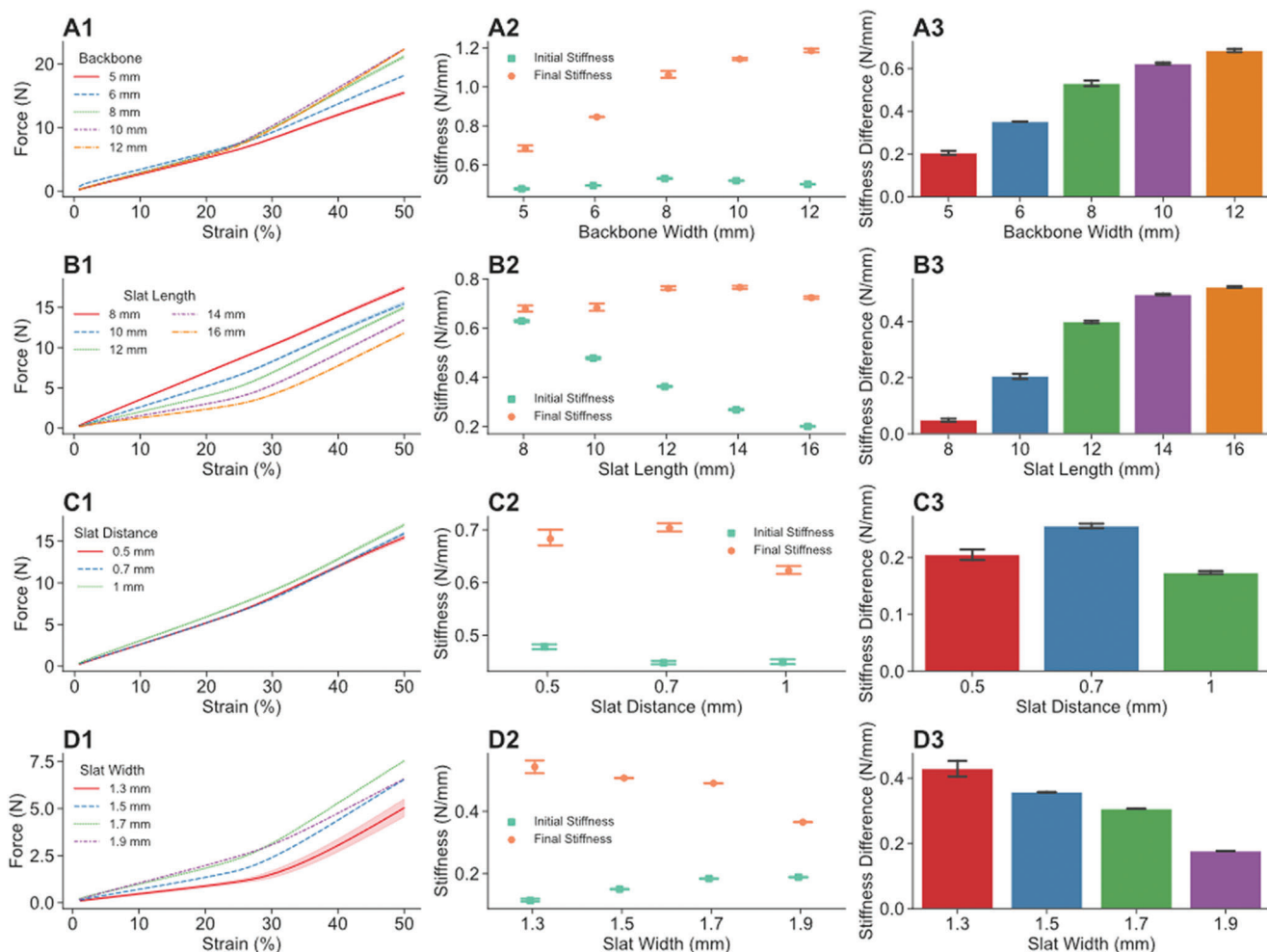


**Figure 3.** Tensile force (N) versus strain (%) (bold curve: average out of 3 curves; shaded area: standard deviation) curve related to PDMS-based samples with different geometry parameters. A) The backbone height strongly influences strain-stiffening, i.e., a large backbone leads to enhanced stiffening. B) Larger slat lengths lead to an increase in the stiffening. A slat length of 8 mm did not lead to a stiffening, as the slats did not touch each other during stretching. C) Slat distance only has a minor effect on strain-stiffening. D) Variations of slat width mainly control the critical strain for strain-stiffening. The plots in the center (A2, B2, C2, and D2) illustrate the average initial and final stiffness of the structures. The graphs to the right (A3, B3, C3, and D3) show the difference between the initial and final stiffness of each unit. The margins of the tensile test curves (left side graphs) and the caps in point plots and bar plots denote standard deviations. For each condition, 3 different samples were measured (3 force curves each).

leads to additional design options for enabling a desired strain-stiffening effect.

In addition, the height of the connection between the two strain-stiffening units in the parallel arrangement can be an additional parameter to adapt. Increasing backbone size between the units in parallel arrangement results in a lower initial stiffness but also a greater final stiffness. This increase in final stiffness due to a thicker backbone is also shown in Figure 4 sample P2, where an increased backbone height, led to no changes in initial stiffness, but to an increase in final stiffness. When putting the strain-stiffening units in series, the slope of the force-elongation curve was decreased and the point of stiffening changed to a higher elongation.

A highly important parameter in strain-stiffening materials is reversibility, as most conventional materials show a strong hysteresis in cyclic tests. We performed cyclic tensile tests to explore this feature as shown **Figure 5**. Hypothetically, the stiffening ef-

fect could be due to the friction between two neighboring slats while being stretched. In order to knock out any possible friction, we have used a lubricant (ZELEC®, Merck, Germany) in the gap between the slats. Interestingly, we did not find a significant difference between the dry sample and the lubricated sample. The cyclic test curves show hysteresis, which is a typical mechanical behavior of silicone-based material.<sup>[22]</sup>

The strain-stiffening materials show a high degree of reversibility in the cyclic test with no evidence of plastic deformation. Due to an initial slip out of the sample of the clamps in the testing machine, only a very slight shift between the first and the other cycles is observed. In addition, there is no significant difference between the lubricated slats and non-lubricated, proving that the friction between the slats does not play a major role in strain-stiffening. This reversibility of strain-stiffening is a clear advantage compared to self-stiffening materials, which is found in certain self-healing materials, where microcapsules of

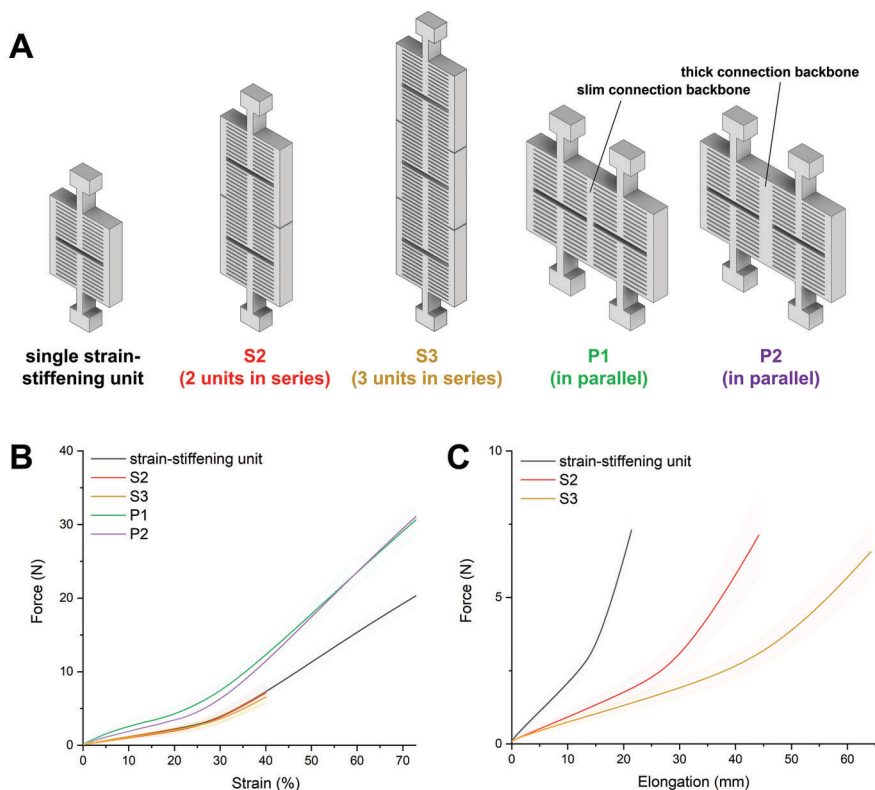


**Figure 4.** Tensile experiments on serial and parallel arrangements of a strain-stiffening unit. A) Design of the arrangement. B) and C) Tensile test results on the PDMS samples sketched in (A) in respect to the applied strain (B) and the elongation (C), demonstrating that a serial arrangement of the strain-stiffening units leads to a decrease of the stiffening effect when elongated the same length, whereas both parallel arrangements lead to a stiffening. For each condition, 3 different samples were measured (3 force curves each, bold curve: average out of 9 curves; shaded area: standard deviation).

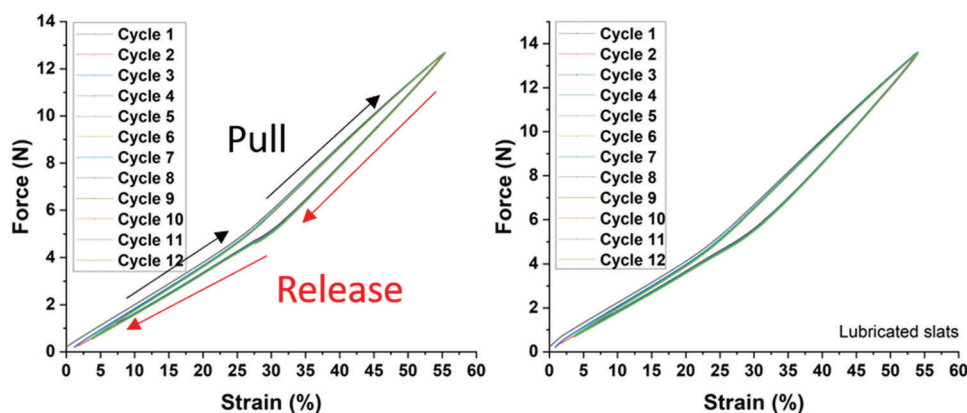


**Figure 5.** Cyclic tensile force (N) versus strain (%) curve. The force-strain-curve shows the reversibility of the strain-stiffening effect in short cycles. The left figure shows the cyclic test up to  $\approx 60\%$  of strain, belonging to the demonstrator sample without using any lubricant between the slats, the right figure includes a lubricant. For each condition, 3 technical repeats were performed.

monomers and catalysts are dispersed in a material.<sup>[23]</sup> The composite can be designed in a way that deformation breaks the embedded capsules and starts the polymerization of the embedded material. If the polymerized embedded material is stiffer than the original material, the material stiffness is increased upon deformation. The downsides are the non-reversibility, as the rupture of the embedded particles and the following polymerization is

not reversible. As speed-independency is an important feature of strain-stiffening and not matched in devices that rely on shear stiffening<sup>[24]</sup>, we also tested our material for three orders of magnitude of stretching speed in tensile tests (Figure 6A). No significant speed dependency is found for initial or final stiffness (Figure 6B). Neither do we observe significant changes over 1000 cycles (Figure S3, Supporting Information).

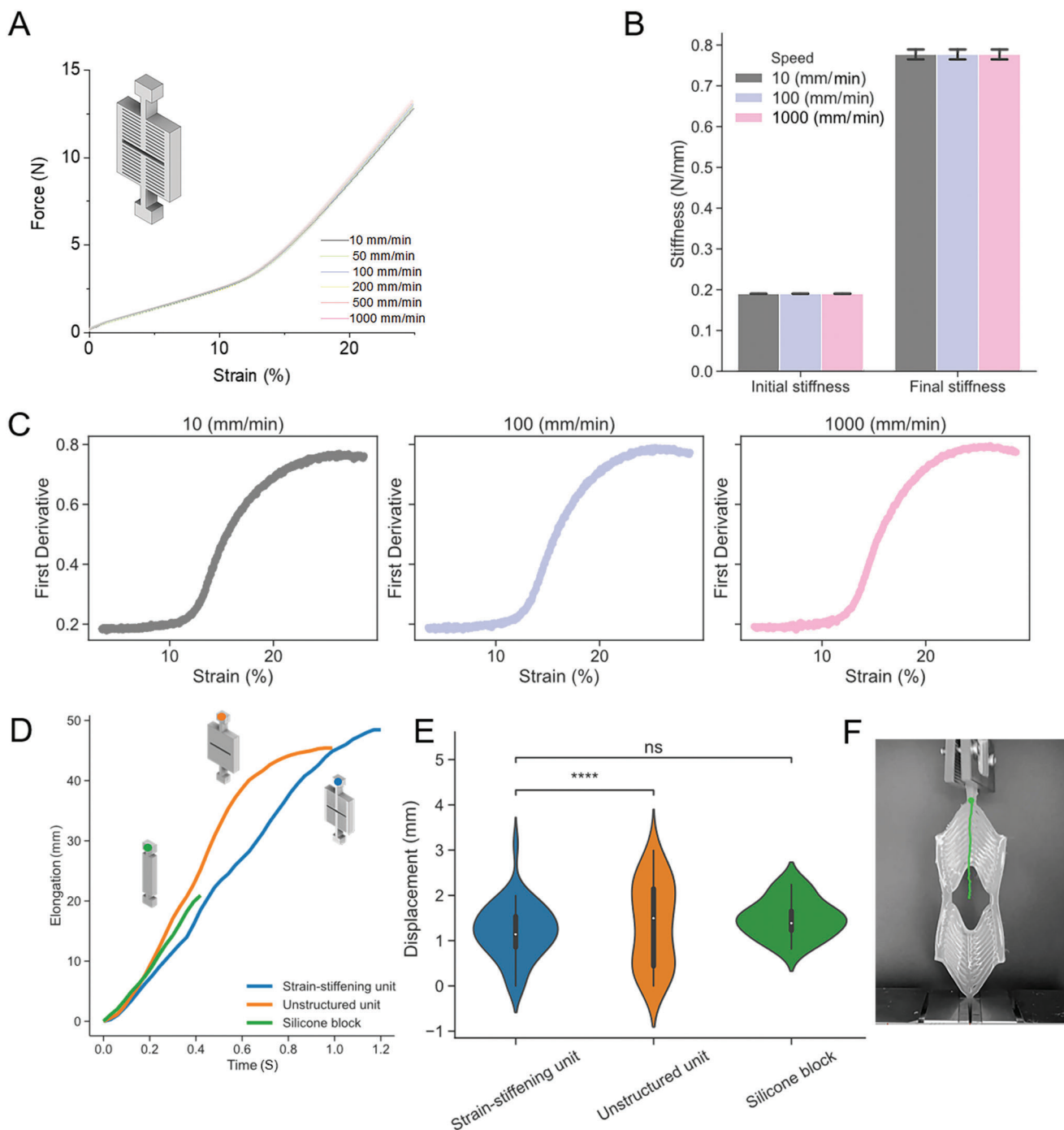


**Figure 6.** Strain-stiffening as a function of stretching speed and analysis of free fall damping. A) Only a tiny speed rate dependency is observed over three orders of magnitude of speed ( $10 \text{ mm min}^{-1}$  to  $1000 \text{ mm min}^{-1}$ ). Each curve is the average out of 3 curves. B) A normalized histogram plot of the material stiffness, stretched at 3 different speed magnitudes ( $10, 100, 1000 \text{ mm min}^{-1}$ ) up to 50% of strain, showing no significant difference of initial and final stiffness. The error bars denote standard deviations. C) Curves obtained by fitting a linear regression function at each 5 points of the force-strain curve. Each data point represents the slope of the linear fit at 3 different speed magnitudes ( $10, 100,$  and  $1000 \text{ mm min}^{-1}$ ) up to 50% of strain. D,F) Damping analysis of the strain-stiffening unit in comparison with other structures by releasing an 1150 g weight and tracking the elongation of each unit from the start of elongation until reaching the maximum elongation. The elongation-time curve (D) shows the damping time for each unit. E) Distribution and dispersion of displacement of the units between frames, i.e. at each time point. The strain-stiffening unit demonstrates a more or less constant displacement whereas in the unstructured unit, the displacement variation is higher suggesting sudden displacement at different time points. The statistical analysis of dispersion was performed by applying Brown-Forsythe test on each pair of units (\*\*\*\*:  $p < 1.00\text{e-}04$ ). (F) The trajectory of this process can be traced in the figure.

Though Yan et al. had received strain-stiffening effects through modifying the matrix material, speed dependency was not discussed and an additional downside is the high-temperature dependency of the strain-stiffening effect of the gels.<sup>[8]</sup> Tran et al. presented gels where the thiol-containing monomers within a poly(ethylene glycol)-acrylate backbone reversibly cross-link upon deformation, causing reversible strain-stiffening of the gel.<sup>[25]</sup> The material stiffens from 150 kPa to 600 kPa in cyclic tension and compression tests. A large downside of this approach is that the stiffening takes several hours. This makes the gels unsuitable for applications where a speed-independent strain-stiffening is desired.

To further investigate the mechanical characteristics of the strain-stiffening units compared to other structures in a realistic scenario, we recorded a series of slow-motion videos of three differently structured units while getting deformed by an 1150 g weight connected to them. As a result, the structured units stretched until they reach a maximum elongation. By tracking the trajectory of the elongation (Figure 6F) for each unit, we could estimate the damping period. As shown in Figure 6D, the strain-stiffening unit has the longest damping period followed by the unstructured unit, and the elongation curve is similar to that of the silicon block unit. The distribution of the displacement vector at each time point between two consecutive frames is significantly less dispersed compared to the unstructured unit (Figure 6E). It indicates a more constrained displacement of strain-stiffening while exerting force on the material that can be damped. Hence, the strain-stiffening unit can also be used to tailor the damping of a free fall.

### 3. Conclusion

Metamaterials provide excellent opportunities to enable mechanical responsivity. This work demonstrates an unconventional, cell-inspired design for such a strain-stiffening metamaterial. Our design and prototypes were mechanically characterized and show that the strain-stiffening effect is tunable, fully reversible, and speed independent. Importantly, the design of the structure can easily be transferred to other elastic materials, as the material matrix is completely unchanged by our approaches. Speed independency is highly important, as it is an important feature in applications, but is typically not found in strain-stiffening materials, which often rely on fibrous networks. Hence, our strain-stiffening metamaterial has broad application potential in the fields of flexible electronics, skin supports and everywhere, where a non-linear, tunable, two-stage mechanical soft response is aimed at.

### 4. Experimental Section

**Sample Preparation:** The samples for the tensile tests were produced from the silicone Elastosil RT625 (Wacker, Germany). Its two components, A and B, were mixed in a 9:1 (w/w) ratio according to the manufacturer's instructions.<sup>[26]</sup> After degassing in a desiccator, the mixture was poured into PLA molds that contained a negative of the final shape. The PLA molds were designed using AutoInventor and printed using Raise3D Pro2 (Raise3D, USA). For a better grip during the tensile tests, T-shaped endings were added to the protrusions. The molds with the pre-polymer mixture were placed in a desiccator to remove trapped air. Then, they were transferred to an oven and cured at 60 °C for one hour. The same geometry of strain-stiffening unit (Table 1) with a slat length of 16 mm was used for the unstructured samples, the arrangement studies, the speed variations tests, and damping experiment. The carbon nanofiber (CNF)-PDMS composite shown in the Supporting Information was prepared by mixing 5 wt.% CNF (Sigma-Aldrich, Germany) with component A for 1 h at 500 rpm with a mechanical stirrer. The rest of preparation was as described above for non-composite PDMS samples.

**Tensile Test:** The tensile tests were conducted using 2.5kN universal tensile test machine (ZwickRoell, Germany). The setup was equipped with a pneumatic grip (ZwickRoell, Germany). A load cell (Xforce 100N, ZwickRoell, Germany) was used to measure the forces. The tensile tests were conducted with a speed of 10 mm min<sup>-1</sup> and up to a strain of maximum 60% in respect to the sample length at the start of the experiment if not stated otherwise. For each test, three samples of the same geometry were measured for 4 cycles. The first cycle was discarded as an initial slipping of the sample in the clamps occurred. To present the results, the 3 curves per sample were combined into one curve by an averaging algorithm in Origin 9.1 (OriginLab, USA) and the average and standard deviation were plotted. The cyclic characterization was measured using the same setup used for the tensile test. In order to knock out possible friction between slats during sample elongation, ≈500 μl of lubricant (ZELECO®, Merck, Germany) was used between each neighboring slats.

The initial and final stiffness of the structures were calculated based on the tensile data. Briefly, the slope of the linear regressions over the initial and final regime was obtained in Python. The initial and final stiffness were plotted as median and standard error (3 technical repeats).

**Damping Test:** The samples were fixed to a clamp at one end and to a rope at the other end. A 1150 g weight was used to deform the structures by pulling on the rope. The weight was released from 20 cm height to exert a momentum to sample once the rope underwent tension. In order to measure the damping behavior, the deformation was recorded at the frame rate of 30 fps with an Apple iPhone. The unfixed ending was tracked using images J software frame by frame and the elongation versus time was recorded.

**Statistics:** The data exported from Zwick tensile test machine presented as mean ± SD, n = 3 using Origin 9.1. The mean values were calculated using the Origin 9.1 mathematic analysis tool "average multiple curves" and plotting the average and standard deviation.

Statistical analysis of dispersion was carried out using Python. To find the significant difference between the elongation variances of the units Brown-Forsythe test was applied on each pair of units (\*\*\*\*: p < = 1.00e-04).

**Supporting Information**

Supporting Information is available from the Wiley Online Library or from the author.

**Acknowledgements**

M. T. and M. S. authors contributed equally to this work. The authors acknowledge the European Research Council through the Proof of Concept Grant VASCUGRAFT, no. 899701. C.S. was supported through the Max Planck School Matter to Life supported by the German Federal Ministry of Education and Research (BMBF). We also thank the Flagship Initiative "Engineering Molecular Systems" funded by the German Federal Ministry of Education and Research (BMBF) and the Ministry of Science Baden-Württemberg within the framework of the Excellence Strategy of Federal and State Governments of Germany. The authors also acknowledge funding by the DFG under Germany's Excellence Strategy 2082/1-390761711 (3D Matter Made to Order) and the Carl Zeiss Foundation, as well as the Volkswagen Foundation through the initiative "Life?" (Az. 96733). We would like to thank Laith Kadem for support with FEM simulations and preliminary tensile test experiments. Special thanks to Trevor Kalkus for English proofreading. Additional thanks to Laura Naumann for helping with the CNF-PDMS composite samples.

### Supporting Information

Supporting Information is available from the Wiley Online Library or from the author.

### Acknowledgements

M. T. and M. S. authors contributed equally to this work. The authors acknowledge the European Research Council through the Proof of Concept Grant VASCUGRAFT, no. 899701. C.S. was supported through the Max Planck School Matter to Life supported by the German Federal Ministry of Education and Research (BMBF). We also thank the Flagship Initiative "Engineering Molecular Systems" funded by the German Federal Ministry of Education and Research (BMBF) and the Ministry of Science Baden-Württemberg within the framework of the Excellence Strategy of Federal and State Governments of Germany. The authors also acknowledge funding by the DFG under Germany's Excellence Strategy 2082/1-390761711 (3D Matter Made to Order) and the Carl Zeiss Foundation, as well as the Volkswagen Foundation through the initiative "Life?" (Az. 96733). We would like to thank Laith Kadem for support with FEM simulations and preliminary tensile test experiments. Special thanks to Trevor Kalkus for English proofreading. Additional thanks to Laura Naumann for helping with the CNF-PDMS composite samples.

Open access funding enabled and organized by Projekt DEAL.

## Conflict of Interest

The authors declare no conflict of interest.

## Data Availability Statement

The data that support the findings of this study are available from the corresponding author upon reasonable request.

## Keywords

cell-inspired materials, elastomers, metamaterials, nonlinear mechanics, strain-stiffening

Received: September 2, 2022

Revised: March 19, 2023

Published online: May 5, 2023

- 
- [1] P. Egan, R. Sinko, P. R. LeDuc, S. Keten, *Nat. Commun.* **2015**, *6*, 7418.
- [2] J. Ohayon, A. M. Gharib, A. Garcia, J. Heroux, S. K. Yazdani, M. Malvè, P. Tracqui, M. A. Martinez, M. Doblare, G. Finet, R. I. Pettigrew, *Am. J. Physiol. Heart Circ. Physiol.* **2011**, *301*, H1097.
- [3] a) H. Joodaki, M. B. Panzer, *Proc. Inst. Mech. Eng. H* **2018**, *232*, 323; b) M. Griffin, Y. Premakumar, A. Seifalian, P. E. Butler, M. Szarko, *J. Vis. Exp.* **2016**, <https://doi.org/10.3791/54872>.
- [4] I. Jorba, G. Beltrán, B. Falcones, B. Suki, R. Farré, J. M. García-Aznar, D. Navajas, *Acta Biomater.* **2019**, *92*, 265.
- [5] Y. Jeong, Y. Yao, E. K. F. Yim, *Biomater. Sci.* **2020**, *8*, 4383.
- [6] T. Wang, M. Wang, L. Yang, Z. Li, X. J. Loh, X. Chen, *Adv. Mater.* **2020**, *32*, 1905522.
- [7] C. Shao, L. Meng, M. Wang, C. Cui, B. Wang, C.-R. Han, F. Xu, J. Yang, *ACS Appl. Mater. Interfaces* **2019**, *11*, 5885.
- [8] B. Yan, J. Huang, L. Han, L. Gong, L. Li, J. N. Israelachvili, H. Zeng, *ACS Nano* **2017**, *11*, 11074.
- [9] W. Zhang, B. Wu, S. Sun, P. Wu, *Nat. Commun.* **2021**, *12*, 4082.
- [10] J. Luo, S. Li, J. Xu, M. Chai, L. Gao, C. Yang, X. Shi, *Adv. Funct. Mater.* **2021**, *31*, 2104139.
- [11] S. R. Deshpande, R. Hammink, F. H. T. Nelissen, A. E. Rowan, H. A. Heus, *Biomacromolecules* **2017**, *18*, 3310.
- [12] Y. Liu, S.-H. Lin, W.-T. Chuang, N.-T. Dai, S.-h. Hsu, *ACS Appl. Mater. Interfaces* **2022**, *14*, 16032.
- [13] J. Cui, J. Chen, Z. Ni, W. Dong, M. Chen, D. Shi, *ACS Appl. Mater. Interfaces* **2022**, *14*, 47148.
- [14] J. Uhlemann, F. Surholt, A. Westerhoff, N. Stranghöner, M. Motevalli, D. Balzani, *Mater. Des.* **2020**, *191*, 108584.
- [15] S. Motte, L. J. Kaufman, *Biopolymers* **2013**, *99*, 35.
- [16] F. Huber, A. Boire, M. P. López, G. H. Koenderink, *Curr. Opin. Cell Biol.* **2015**, *32*, 39.
- [17] K. Burrige, E. S. Wittchen, *J. Cell Biol.* **2013**, *200*, 9.
- [18] a) S. Lin, X. Han, G. C. P. Tsui, D. Hui, L. Gu, *Compos. B. Eng.* **2017**, *116*, 377; b) S. Na, G. A. Meiningner, J. D. Humphrey, *J. Theor. Biol.* **2007**, *246*, 87; c) S. Tavares, A. F. Vieira, A. V. Taubenberger, M. Araújo, N. P. Martins, C. Brás-Pereira, A. Polónia, M. Herbig, C. Barreto, O. Otto, J. Cardoso, J. B. Pereira-Leal, J. Guck, J. Paredes, F. Janody, *Nat. Commun.* **2017**, *8*, 15237.
- [19] M. Yoshigi, L. M. Hoffman, C. C. Jensen, H. J. Yost, M. C. Beckerle, *J. Cell Biol.* **2005**, *171*, 209.
- [20] S. Tojkander, G. Gateva, P. Lappalainen, *J. Cell Sci.* **2012**, *125*, 1855.
- [21] a) M. Timmermann, N. Lukat, L. P. Schneider, C. W. Shields, G. P. López, C. Selhuber-Unkel, *ACS Biomater. Sci. Eng.* **2020**, *6*, 889; b) S. B. Gutekunst, C. Grabosch, A. Kovalev, S. N. Gorb, C. Selhuber-Unkel, *Beilstein J. Nanotechnol.* **2014**, *5*, 1393.
- [22] A.-M. M. R. Persson, E. Andreassen, *Polymers* **2022**, *14*, 1316.
- [23] R. S. Trask, H. R. Williams, I. P. Bond, *Bioinspiration & Biomimetics* **2007**, *2*, P1.
- [24] C. Zhao, X. Gong, S. Wang, W. Jiang, S. Xuan, *Cell Rep. Phys. Sci.* **2020**, *1*, 100266.
- [25] Y. H. Tran, M. J. Rasmuson, T. Emrick, J. Klier, S. R. Peyton, *Soft Matter* **2017**, *13*, 9007.
- [26] <https://www.wacker.com/h/de-de/medias/ELASTOSIL-RT-625-AB-de-2022.02.23.pdf> (accessed: 08, 2022).